AIAA Journal

VOLUME 3 MAY 1965 NUMBER 5

Interaction of a Shock Wave and a Wedge: An Application of the Hydraulic Analogy

ENRIQUE J. KLEIN*
The Royal College of Science and Technology,† Glasgow, Scotland

A study is made, using the hydraulic analogy to compressible gas flow, of the two-dimensional flow patterns for 1) a strong shock wave striking a wedge in supersonic motion which has weak attached shocks, 2) a weak shock wave striking a wedge in supersonic motion which has strong attached shocks, and 3) a strong shock wave striking a stationary wedge at varying angles of incidence. Experimental hydraulic flow patterns are compared with theoretical aerodynamic features, where these exist, showing good over-all agreement. Experimental transient flow field distributions along the model wall are obtained for case 2. These results are interpreted as density distributions for the corresponding aerodynamic case through a theoretical correlation and are compared with results from a linearized theory. The experimental reproduction process and techniques are presented, and a description is given of the hydraulic analogy tank used.

Nomenclature

(Fr)	=	Froude number
h	=	water depth in open channel
L	=	length
l	=	coordinate in the direction of the x axis
(Ma)	=	Mach number
x	=	axis along the flow deflecting wall
γ	=	ratio of specific heats
θ	=	angle of flow deflection, positive for compression flow and negative for expansion flow
ρ	=	density
ψ	=	angle between the attached discontinuity and the initial direction of motion

Subscripts

1, 2, . . . , 5	=	denote steady-state regions in the flow pattern, see inset of Fig. 10.
0	=	denotes primary upstream conditions
θ	=	denotes secondary upstream conditions
comp	=	denotes compression
exp	=	denotes expansion

Received August 3, 1964; revision received January 18, 1965. This investigation forms part of a Ph.D. thesis entitled "The hydraulic analogy to high speed gas flow," presented by the author to the University of Glasgow, in October 1963. The author wishes to express his grateful appreciation to A. S. T. Thomson, Head, Division of Mechanical, Civil, and Chemical Engineering, The Royal College of Science and Technology, for his continued support, and to D. C. Pack, Head, Department of Mathematics, for his interest in the investigations and his discussion of this paper. The author thanks W. Anderson, Lecturer, for making available unpublished theoretical results.

* Graduate Student; now Research Engineer, Mechanics Department, Physics Division, Stanford Research Institute, Menlo Park, Calif.

† Now The University of Strathclyde.

Introduction

THE most important asset of the hydraulic analogy is its capability of reproducing the features of two-dimensional compressible flows. This is useful since it makes possible the verification of some of the basic assumptions about flow patterns, which are necessary in the development of theoretical solutions.

The hydraulic analogy to compressible gas flow has been applied in the past to a wide variety of problems in gasdynamics, and an extensive literature exists on the subject. A general background can be obtained from a very complete series of studies on the validity and applicability of the hydraulic analogy, carried out at the Massachusetts Institute of Technology by Ippen, Harleman, and Crossley.[1]

It has been shown in the derivation of the basic equations that the analogy holds for two-dimensional, ideal, unsteady flow. With continuous flow the analogy only provides exact agreement with a gas having $\gamma = 2$, and with flow containing discontinuities, the shock wave system is not strictly analogous to the hydraulic jump system. Nevertheless, the hydraulic analogy has never failed to reproduce qualitatively the gasdynamic features, so it is permissible to apply this technique to the study of transient shock interaction and diffraction problems. The limitations to the quantitative agreement of the analogy make necessary the development of theoretical correlations, which establish an analytical relationship between corresponding hydrodynamic and aerodynamic quantities so as to make other variables equivalent.

The main restrictions to the application of the analogy can be summarized as follows. It can only be applied to one- or two-dimensional cases. The analogy equations hold strictly only for the ideal, isentropic flow of a gas with $\gamma = 2$ and are not valid when discontinuities occur. Real fluid

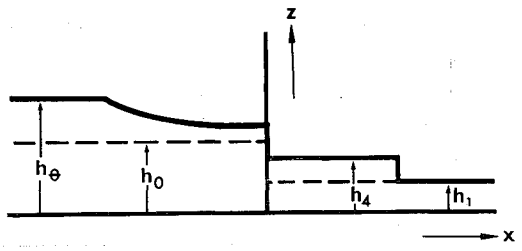

Fig. 1 Release of an advancing hydraulic jump. h_1 = depth of the initial flow, h_4 = depth behind the incident hydraulic jump, h_0 = primary upstream head, and h_θ = secondary steady-state upstream head.

effects, which are not considered in establishing the analogy equations, are of a different nature in the two types of flow. Certain effects present in the hydraulic case have no counterpart in the gaseous case. These include the bottom flow boundary layers; capillary waves; the periodicity of gravity waves; the existence of two types of hydraulic jumps, undular and regular; and the large thickness of the jump front.

The experimental investigation of the first two interaction cases presented in this paper would be extremely difficult in a gaseous medium, requiring expensive equipment and very complex techniques. Therefore, the hydraulic analogy, in spite of its many limitations, provides the most effective and perhaps the only practical method available. The simplification with the hydraulic analogy occurs mainly because the ratio of the velocity of sound in air to the velocity of propagation of gravity waves in shallow water, which are correspondent, is of the order of 1000:1, slowing down the entire transient process. Experimental equipment and new techniques were developed for this investigation.

Experimental Reproduction of the Interaction Cases

Three cases of the two-dimensional interaction of a shock wave and a wedge are investigated:

1) An infinite wedge moving at constant supersonic velocity in an undisturbed medium, with weak attached shocks: Its velocity vector is parallel to its axis of symmetry. The wedge is struck by a strong, plane shock advancing into the undisturbed medium along the same lines of motion as the wedge but in the opposite direction.

2) An infinite wedge moving at constant supersonic velocity in an undisturbed medium, with strong attached shocks: Its velocity vector is parallel to its axis of symmetry. The wedge is struck by a weak, plane shock advancing into the undisturbed medium along the same lines of motion as the wedge but in the opposite direction.

3) An infinite wedge lying stationary in an undisturbed medium: The wedge is struck by a strong plane shock, incident at varying angles of approach.

To reproduce the conditions of flow for cases 1 and 2 by the hydraulic analogy technique, the model is kept stationary with a shallow flow of water past it. A plane hydraulic jump is then released into the initial flow. This rearrangement of relative velocities is only possible since the wedge and the incident jump are required to move along the same lines of motion.

The conditions of flow for case 3 are obtained by making a hydraulic jump travel into still shallow water in which the stationary model has been positioned at the required angle. Varying the angle of the model instead of the angle of the incident jump is permissible since the model and its surrounding medium are initially at rest.

For cases 1 and 2, the method used to produce the incident hydraulic jump is similar to the method used to produce an incident shock wave in a constant section shock tube. In a shock tube, a diaphragm between two chambers of different state is ruptured, releasing a shock, which travels into the low-pressure region associated with a rarefaction propagating into the high-pressure region. Similarly, in the hydraulic analogy tank the rapid release of an additional sluice between two sections of different levels causes a hydraulic jump to travel downstream and a depression to travel upstream of the sluice gate system, Fig. (1). The flow behind the jump is of a steady nature as long as no reflection of the depression occurs upstream. There are two fundamental differences between the present hydraulic analogy experiment and a constant section shock-tube experiment: whereas initially in the shock tube the high-pressure chamber is completely cut off from the low-pressure chamber by the diaphragm, in the hydraulic analogy tank there is a steady flow from the upstream reservoir to the test section under a partly raised sluice; and further, whereas in the shock tube the rupture of the diaphragm opens up the full section between both chambers, the release of an additional sluice in the hydraulic analogy tank opens only part of the equivalent section. For case 3, the traveling hydraulic jump is obtained by a technique equivalent to producing a shock wave in a still uniform medium.

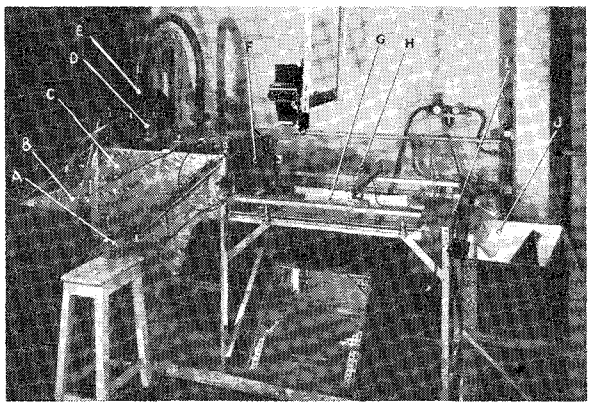

Fig. 2 The hydraulic analogy tank. A = compressed air system. B = overflow tank. C = main reservoir. D = vacuum connection. E = inlet pipe arrangement. F = main sluice gate. G = test section. H = measuring carriage. I = exit weir. J = sump tank.

Description of the Equipment

The hydraulic analogy tank designed by the author and used for this set of experiments is shown in Fig. 2. The equipment was designed as a closed loop with a recirculating system. To avoid the transmission of vibrations from the pumping system to the test section G, the overflow tank B, and the sump tank J are completely detached from the frame of the main tank. The water inlet pipe arrangement E, also has no contact with the main reservoir C.

In the circulating system, the pump conveys the water through a throttling valve, a Venturi-tube, and the inlet pipe arrangement E, into the main reservoir C. There the water is kept at a constant level with the help of an overflow weir discharging into the overflow tank B, with a thin sheet of water flowing under the main sluice gate F, onto the test section G. From there the water flows over the exit weir I, into the sump tank J. The sump tank and the overflow tank are connected by a level equalizing pipe, and the pump suction is connected to the sump tank, thus completing the loop. The test section is 24 in. wide by 40 in. long and has a glass floor to permit the illumination of the flow from below.

Additional equipment is required to produce the advancing hydraulic jump. This consists of a jump release mechanism, an overflow shutoff sluice, a vacuum enclosure with a vacuum breaking mechanism, and a compressed air operating system. The jump release mechanism consists of an additional sluice attached to the main sluice gate, which can be rapidly lifted.

The overflow shutoff sluice operates on top of the overflow weir. The top of the main reservoir is enclosed to permit making a partial vacuum over the water surface. This enclosure is provided with a vacuum breaking mechanism. All the previously mentioned devices for the production of the advancing jump are operated simultaneously by a compressed air system.

Experimental Techniques

A steady, uniform flow over the test section is produced by having a sheet of water flowing onto the test section from under the partly raised main sluice gate. The necessary head to produce this flow is maintained in the main reservoir by the constant discharge of the pump. The settings required to obtain these flow conditions are the discharge of the pump, the main sluice gate setting, and the test section slope.

A hydraulic jump advancing into steady flow is produced as follows. Primary steady flow conditions are obtained with the pump discharge set for the secondary flow conditions. The primary flow is produced by operating with the additional sluice interposed, part of the pump discharge going over the overflow weir, and the water in the main reservoir under vacuum. The physical water level in the main reservoir corresponds to the effective head required under atmospheric pressure to produce the secondary flow behind the advancing jump. To produce the secondary flow, the additional sluice controlling the primary flow is lifted. At the same time the vacuum in the main reservoir is broken, and the overflow shutoff sluice is interposed. This causes the rapid transition from the primary to the secondary depth of flow, the primary effective head in the main reservoir to the secondary effective head, and the primary to the secondary discharge over the test section. The settings required to obtain these flow conditions are the pump discharge, the vacuum setting, the main sluice gate setting, the additional sluice setting, the overflow weir setting, and the test section slope.

To produce a hydraulic jump advancing into stationary water, a stationary layer of water is formed over the test section set at zero slope with a continuous surface with the water in the main reservoir. The total pump discharge is made to flow across the overflow weir. To produce the transient flow, the overflow shutoff sluice is interposed, suddenly diverting the flow into the test section and causing the advancing hydraulic jump. The settings required to obtain these conditions are the pump discharge, the exit weir, and the overflow weir.

Various measuring and recording techniques were used. The total discharge from the pump is measured from a mercury column manometer connected to a Venturi-tube. The main reservoir water depth is measured by a probe with a vernier scale. Steady depths of flow over the test section are measured by a micrometer depth gage mounted on an orthogonal displacement rig. Measurement of transient depths is made by a capacitance proximity meter connected to an oscilloscope with a filming recorder. Velocities of steady flow are determined from photographic double exposures of stroboscopically illuminated particles of foil floating on the water, and the velocity of the incident jump, by illuminating the jump front itself in the same manner.

The photographic technique employed to obtain flow pattern configurations is the shadowgraph method. This consists in illuminating the flow pattern from below through the transparent glass floor of the test section, then photographing from above the image cast on a ground glass sheet suspended over the flow.

Interaction Flow Patterns

A series of experiments were carried out to determine the flow patterns for the three different cases of the interaction process.

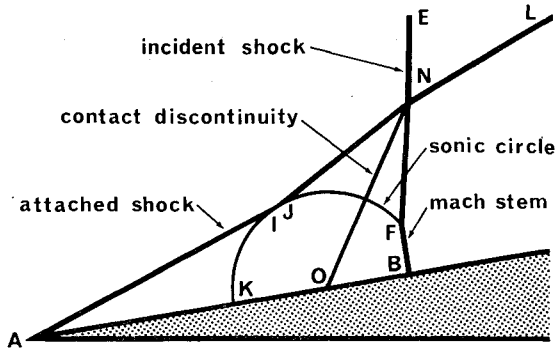

Fig. 3 Schematical interaction pattern in gas: weak attached shock, strong incident shock.

Case 1

The parameters for the aerodynamic problem are the flow deflection angle θ, the primary Mach number $(Ma)_1$, and the strength of the incident shock given by the ratio of densities across it ρ_4/ρ_1. The corresponding hydrodynamic quantities are the flow deflection angle θ, the primary Froude number $(Fr)_1$, and the strength of the incident jump given by the ratio of depths across it h_4/h_1.

The schematical configuration of Fig. 3 corresponds to the experimental hydraulic flow pattern of Fig. 4. It is used for comparison with theoretical aerodynamic features. The lower wall of the model in Fig. 4 is parallel to the direction of flow. Since the pattern would be symmetric for a complete wedge and the upper flow independent of the lower flow, it is sufficient to consider one side only.

The theoretical features for this case were given by Smyrl.[2] All regions in Fig. 3 are of constant state except that bounded by the sonic circle and the segment FB. The line $ENFB$ represents the shock front advancing from left to right. The straight segment EN is not affected by the interaction. NF is also straight but forms a small angle with the vertical, away from the leading edge. At the triple point F the shock curves and ends up at B normal to the deflecting wall forming a Mach stem. The segment NL is part of the original attached oblique shock. The straight segment AJ corresponds to the new attached shock and is tangent to the sonic circle $FJIK$. The oblique shock is completed by the segment IN, also tangent to the sonic circle. The angle of the new attached shock differs from the angle of the original attached shock because the Mach numbers in front and behind the strong incident shock are different. The sonic circle is originated at the leading edge by the incidence of the advancing shock. A contact discontinuity runs from O to N, separating the air which crossed EN from region ENL and

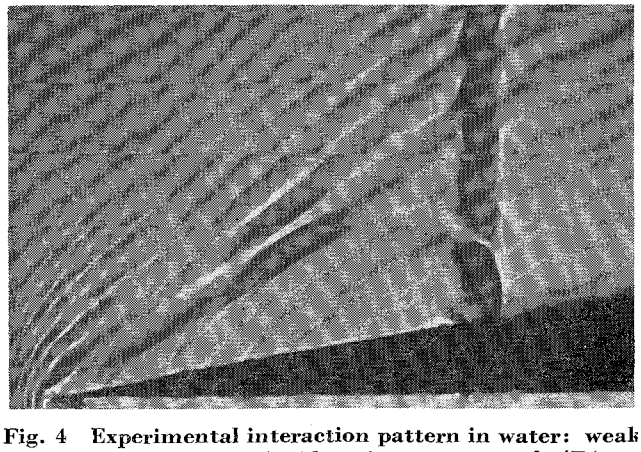

Fig. 4 Experimental interaction pattern in water: weak attached jump, strong incident jump; $\theta = 10°$, $(Fr)_1 = 2.5$, $h_4/h_1 = 1.4$, $h_1 = 0.165$ in.

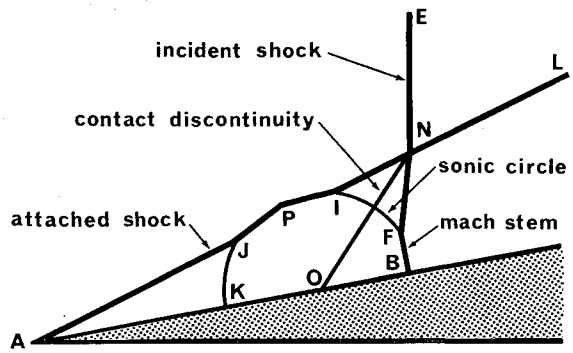

Fig. 5 Schematical interaction pattern in gas: strong attached shock, weak incident shock.

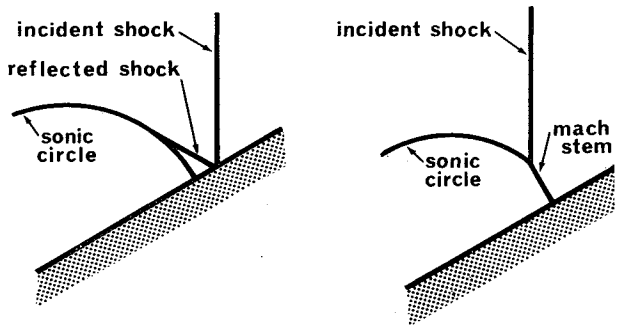

Fig. 7 Regular reflection of a shock wave at a deflecting wall (left), and Mach reflection of a shock wave at a deflecting wall (right).

then entered the disturbance zone ONA from the air which crossed NB directly from the region bound by LNB and the wedge wall, into the region OBN.

In the experimental flow pattern of Fig. 4, the incident jump shows clearly a perpendicular approach at the deflecting wall and a bend starting at the intersection with the largest disturbance circle. Between the leading edge of the model and the incident jump, the attached oblique jump, the one nearest the deflecting wall, has two straight segments tangential to a circular disturbance zone. The intersection of the two straight segments is outlined more sharply indicating a strengthening in that region. The undisturbed sections of the original attached jump and of the incident jump remain unaltered. A check using high-speed filming showed that the interaction pattern remains geometrically steady during the passage of the incident jump. It is interesting to observe that the centers of the circular disturbances inside the circular-disturbance region are distributed along the model wall, those corresponding to the smaller disturbances being nearer the incident jump. These disturbances are created continuously by the end of the incident jump moving along the model wall. The lag occurs since the velocity of the jump is greater than that of the flow behind it. A strong point disturbance next to the model wall and the incident jump, which was not predicted theoretically, can be seen in Fig. 4. It is tentatively suggested that this corresponds to a breaking up of the foot of the incident jump caused by its interaction with the boundary layer at the model wall. All waves outside the main attached jump are capillary waves. On the other hand two of the theoretical features are not apparent in the experimental pattern. The section of the incident jump inside the attached jump shows a slight deflection toward the leading edge of the model and not away from it. This becomes more noticeable in photographs showing the interaction pattern at a later stage of development. The contact discontinuity ON is not visible in the hydraulic flow pattern. Since contact discontinuities are not associated with a pressure, density, or absolute temperature discontinuity, they do not appear as jumps in the hydraulic flow and are therefore not directly visible. For the same reasons contact discontinuities do not appear in the experimental flow patterns of cases 2 and 3.

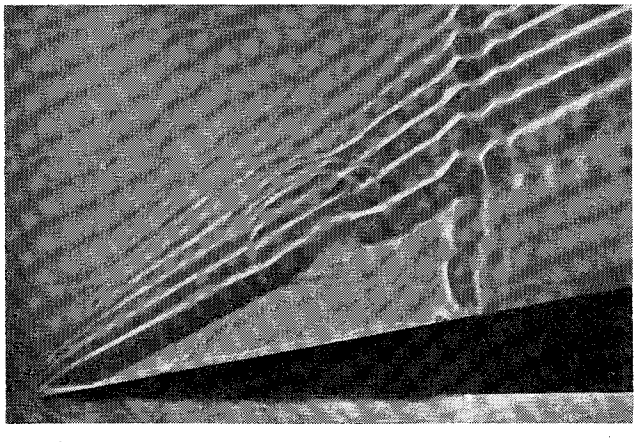

Fig. 6 Experimental interaction pattern in water: strong attached jump, weak incident jump; $\theta = 10°$, $(Fr)_1 = 3.3$, $h_4/h_1 = 1.2$, $h_1 = 0.250$ in.

Case 2

The configuration of Fig. 5 shows schematically the experimental flow pattern of Fig. 6. The parameters of flow are the same as for case 1, and the flow pattern is basically similar too. The theoretical assumptions for this case were put forward by Anderson.[3] Some features differ from those of case 1. For a very weak incident shock (sound pulse), the straight segment NF is inclined toward the leading edge. Its end extends up to the wall of the wedge, and its reflection terminates tangent to the sonic circle, as shown in Fig. 7 (left). The new attached shock AJ and the segment IN intersect the sonic circle at J and I, respectively. A sharp bend is predicted around the center of the section JI, with approximately straight approaches, continuous at J and I with the segments AJ and IN. The angle of the new attached shock varies only slightly from the angle of the primary shock, since the difference between the Mach numbers in front and behind the weak incident shock is small.

The experimental flow pattern of Fig. 6 shows that the incident jump inside the attached jump bends slightly toward the leading edge. This becomes more apparent as the strength of the attached jump is increased with respect to the strength of the incident jump. The segment bends again at the intersection with the disturbance circle, and ends normally at the model wall forming a Mach stem. A shadow between the incident jump and the attached jump indicates the presence of the disturbance circle. The attached jump shows two straight segments forming an angle at a position where the circular disturbance intersects the attached jump. A slight weakening can be detected in the region of intersection of the two segments. A short straight line starting from the first break in the attached jump, approximately parallel to the initial direction of flow, can also be observed. The line is followed by a patch disturbance. The angle of the attached jump is hardly altered by the passage of the incident jump. The intermittent disturbance to the right of the intersection of the incident and the attached jumps also appears in the initial steady flow and has no relation to the interaction. The waves outside the main attached jump, including the circular ripples, are caused by capillary effects. As in case 1, the incident jump tends to dissipate next to the model wall. Also it can be observed that the weak incident hydraulic jump tends to break up into successive smaller jumps. The main divergence between the

theoretical predictions and the experimental results is the occurrence of a Mach type reflection of the incident jump at the model wall. This is a consequence of the comparatively large strength of the incident jump and small angle of flow deflection used in the experiment. In the experimental shock configuration, bends occur at points J and I on the attached jump, whereas theoretically only a sharp kink in the central part of section JI is predicted.

Case 3

The parameters for the aerodynamic problem are the compression flow deflection angle θ_{comp}, the expansion flow deflection angle θ_{exp}, and the strength of the incident shock given by the density ratio ρ_4/ρ_1. The corresponding hydrodynamic quantities are θ_{comp}, θ_{exp}, and h_4/h_1.

The schematical flow pattern of Fig. 8 corresponds to the experimental results of Fig. 9b. The theoretical features for this case are summarized mainly from Fletcher, Taub, and Bleakney.[4] The line EFB represents the incident shock on the compression flow side, and $B'E'$ on the expansion flow side. The straight segment EF is not affected by the diffraction of the shock. The incident shock bends at the triple point F and terminates at B on the deflecting wall, forming a Mach stem, which is generally curved. Mach reflections of the incident shock occur with small flow deflection angles. As the angle is increased beyond a given limit, the reflection becomes of the regular type. A reflected shock starts from the triple point F and gradually curves around the leading edge. A contact discontinuity is predicted along the path of the triple point OF. The incident shock on the expansion flow side curves, terminating normal to the wall. The flow behind the incident shock is supersonic, whereas the flow bounded by the reflected shock in the upper region can be subsonic or supersonic depending on the magnitude of the flow deflection angle and the strength of the incident shock. When the flow is supersonic, the initial section of the reflected shock, starting at F, is straight; whereas for subsonic flow it is curved over its entire length. An expansion zone that occurs around the leading edge of the wedge is described by Guderley.[5] A sonic line, originating at the leading edge normal to the upper wall, curves from the compression side to the expansion side of the wedge and envelopes the expansion zone at the leading edge. This expansion zone is followed by a flow separation region along the lower wall. Beyond the sonic line and behind the incident shock on the lower side, the flow is supersonic.

The photographs of Figs. 9a, 9b, and 9c show the resulting flow pattern for a 10° wedge with its compression side at 15°, 30°, and 45° to the direction of travel of the incident jump. The experimental patterns show that the hydraulic equivalent of a Mach stem occurs on the compression side. This segment becomes shorter as the deflection angle is increased, and almost a regular reflection occurs with θ_{comp} = 45°. It also shows a marked curvature for the case of θ_{comp} = 15°, and less curvature for θ_{comp} = 30°. The reflected wave curves around the leading edge of the model and becomes weaker as it approaches normally the lower section of the incident jump. The strength of this reflected wave also increases with increasing θ_{comp}. The formation of circular disturbances with the passage of the incident jump can be observed as in the experimental pattern for case 1. The incident jump on the expansion side curves toward the leading edge of the model and goes through an inflection point before ending at right angles to the model wall. An expansion zone around the leading edge, followed by a flow separation on the lower wall of the model, are clearly apparent. The expansion zone is apparent for the cases of θ_{comp} = 15°, 30°, and 45°, whereas the flow separation only seems to be present for θ_{comp} = 30°, 45°. In the flow patterns of Figs. 9a, 9b,

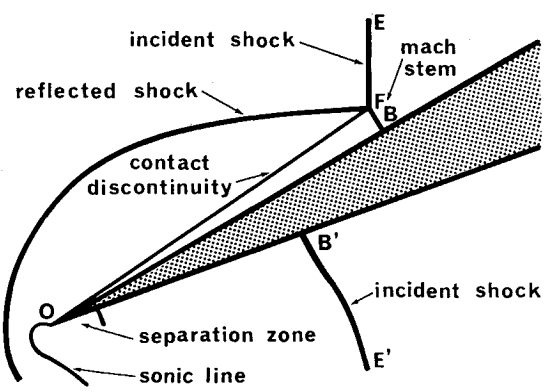

Fig. 8 Schematical diffraction pattern in gas: stationary wedge, strong incident shock

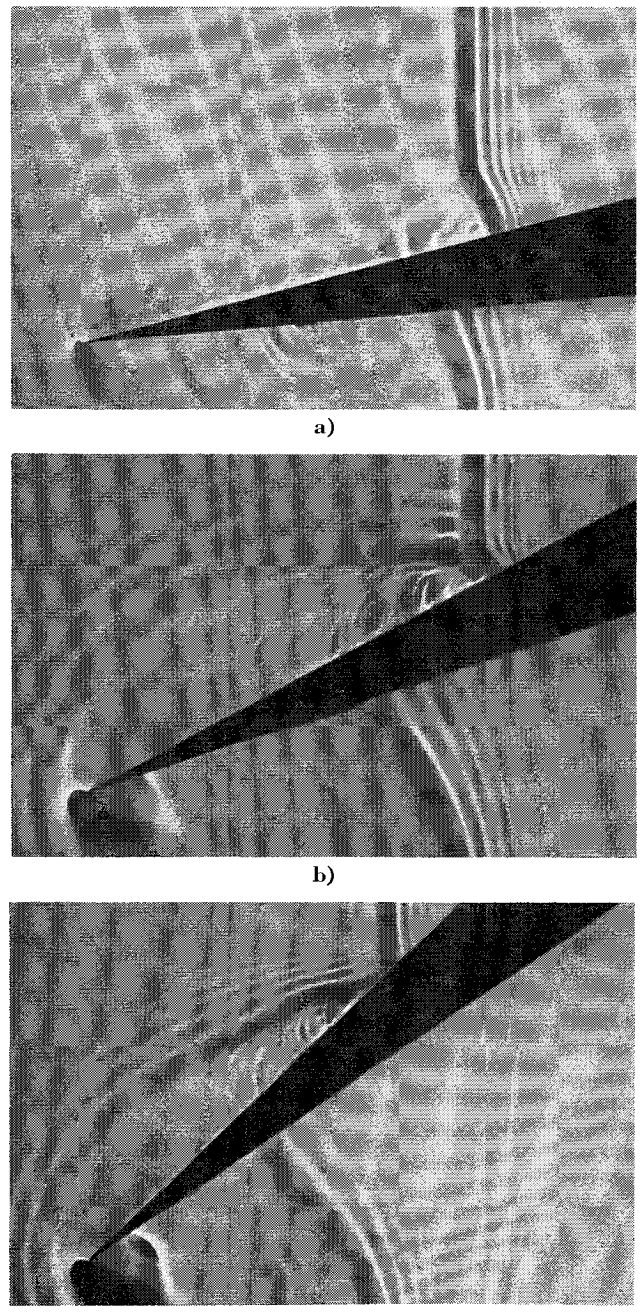

Fig. 9 Experimental diffraction pattern in water: stationary wedge, strong incident jump; wedge angle = 10°, h_4/h_1 = 1.8, h_1 = 0.250 in. a) θ_{comp} = 15°, θ_{exp} = − 5°; b) θ_{comp} = 30°, θ_{exp} = − 20°; c) θ_{comp} = 45°, θ_{exp} = −35°.

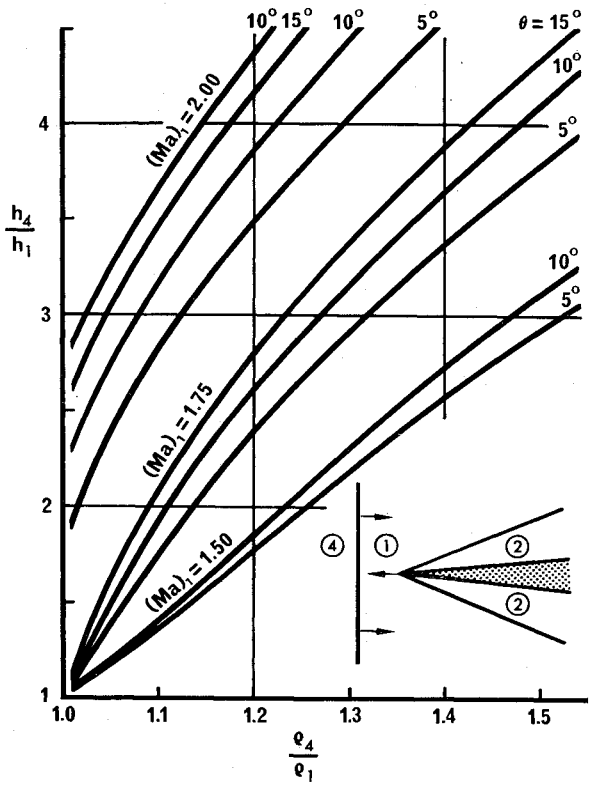

Fig. 10 Correlation curves for the aerodynamic and hydrodynamic cases of the interaction problem.

and 9c capillary waves appear in front of the incident jump as well as outside the reflected jump.

Flow Field Distribution

The aerodynamic density distribution along the deflecting wall, resulting from the transient interaction process with the incident shock, is determined from the experimental hydraulic flow results.

Since the exact analogy breaks down with the occurrence of shock waves, to derive quantitative aerodynamic information from hydraulic analogy experimental work, a theoretical correlation for this case must be established to account for the divergence between the aerodynamic and hydrodynamic equations.

An approach by Ippen and Harleman[1] provides a theoretical exact analogy between water depth and air density ratios, as well as geometry of flow for steady flow across a single straight oblique discontinuity produced by a straight flow deflection. An extension of this correlation to the present case, requires that the correlation applied to the initial flow should be equally valid for the resulting final steady flow. A theoretical correspondence is then established between the depth and density ratios across the oblique discontinuity separating steady flow regions, as well as for the steady geometries of flow, i.e., flow deflection angle, and shock and jump angle, before and after the interaction with the plane incident discontinuity.

Regions of unsteady flow also occur in the transient interaction process. No exact correlation is possible in these regions, and the classical analogy laws apply.

The correlation is based on an equivalence of water depth ratios to air density ratios rather than on pressure or absolute temperature ratios because it has been shown[1] that, after the breakdown of the classical analogy with the appearance of shock waves, the curves of density ratio across a shock in air provide the closer agreement with the curves of depth ratio across a hydraulic jump in water. In the evaluation of the results from the hydraulic analogy in the unsteady region, the best approach consists in interpreting water depth ratios directly as density ratios in air.[1]

The establishment of the correlation requires the solution of a system of simultaneous equations based on the following:

$$\frac{\rho_2}{\rho_1} = \frac{2.4(Ma)_1^2 \sin^2\psi_1}{0.4(Ma)_1^2 \sin^2\psi_1 + 2} \tag{1}$$

$$\rho_2/\rho_1 = \tan\psi_1/\tan(\psi_1 - \theta) \tag{2}$$

$$\frac{(Fr)_1}{(Ma)_1} = \left[\frac{(1 + \rho_2/\rho_1)(6 - \rho_2/\rho_1)}{10}\right]^{1/2} \tag{3}$$

$$(Ma)_4 = \left[5\frac{(\rho_4/\rho_1 - 1)(1 - \rho_1/\rho_4)}{(6 - \rho_1/\rho_4)}\right]^{1/2} + \left[\frac{6 - \rho_4/\rho_1}{6 - \rho_1/\rho_4}\right]^{1/2} (Ma)_1 \tag{4}$$

$$(Fr)_4 = \left[\frac{1}{2}\left(1 + \frac{h_4}{h_1}\right)\right]^{1/2}\left(1 - \frac{h_1}{h_4}\right) + \left(\frac{h_1}{h_4}\right)^{1/2} (Fr)_1 \tag{5}$$

In Eqs. (1, 3, and 4), $\gamma = 1.4$. The subscripts correspond to the regions in the flow field shown in the inset of Fig. 10. Equation (1) is the density ratio across an oblique shock in air obtained from the Rankine-Hugoniot relationship. Equation (2) is the same density ratio derived from geometrical and continuity considerations. Equation (3) is the Ippen and Harleman equation obtained from the conditions for the correlation. Equation (4) represents the Mach number behind an incident shock derived from the mass and momentum conditions. Similarly Eq. (5) represents the Froude number behind an incident hydraulic jump.

The system of simultaneous equations is formed by the preceding plus Eqs. (1, 2, and 3) applied to the steady conditions after the passage of the incident shock, i.e., subscript 1 replaced by 4, and subscript 2 replaced by 5. The correlation then requires that $\rho_2/\rho_1 = h_2/h_1$, $\rho_5/\rho_4 = h_5/h_4$, $\psi_{1\text{air}} = \psi_{1\text{water}}$, $\psi_{4\text{air}} = \psi_{4\text{water}}$, and $\theta_{\text{air}} = \theta_{\text{water}}$. The system is solved by numerical methods to give the depth ratio across the incident hydraulic jump h_4/h_1, as a function of ρ_4/ρ_1, the density ratio across the incident shock, with θ and $(Ma)_1$ as parameters. The results are shown in the graph of Fig. 10.

It can be seen from the graph that the correlation restricts hydraulic analogy experimental work to the representation of relatively weak incident shocks in air, since h_4/h_1 increases very rapidly with increasing ρ_4/ρ_1. At the same time this provides a natural amplification for the gaseous case, which is very favorable for the determination of results. It is also interesting to note that, as $(Ma)_1$ is increased, the correlation starts breaking down below increasing values of h_4/h_1.

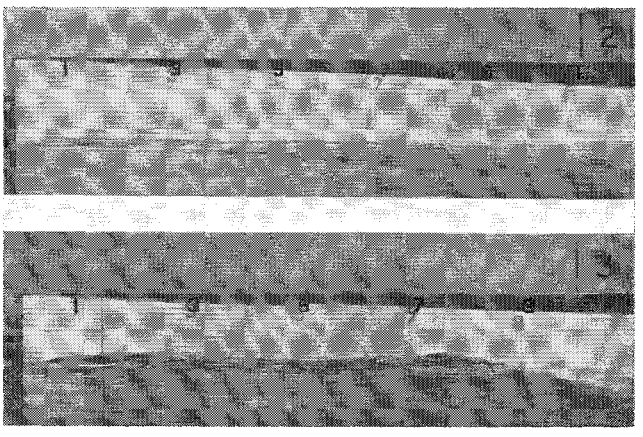

Fig. 11 Water depths along the model wall with steady flow (above), and transient depths caused by the incident hydraulic jump (below).

The interaction case considered is that of a weak shock striking a supersonically traveling wedge with strong attached shocks, i.e., case 2. The theoretical solution studied by Anderson[3] provides a comparison for the experimental results of this investigation. Theoretical results are obtained in the form of nondimensional pressures along the straight deflecting wall and are transformed into nondimensional density distributions.

The experimental results are obtained in the form of depth distributions along the model wall, as in Fig. 11 (lower). These depth distributions when made nondimensional can be directly interpreted as nondimensional density distributions because the correlation between the aerodynamic and hydrodynamic cases is applied.

The choice of the aerodynamic data was mainly conditioned by the requirements of the existing theory and the restrictions imposed by the experimental technique. The aerodynamic data was taken as $(Ma)_1 = 1.85$, $\rho_4/\rho_1 = 1.10$, and $\theta = 10°$. The corresponding hydrodynamic quantities obtained through the correlation are $(Fr)_1 = 1.951$, $h_4/h_1 = 2.3366$, and $\theta = 10°$.

Experiments were conducted with a 28-in. chord, 5° angle half-diamond model. The surface tension of the water was lowered to 41.6 dynes/cm by the addition of a detergent. A silicone emulsion was also added to reduce foam formation and give the water uniform nonwetting properties. This gave excellent results in reducing the meniscus formation at the model wall. The slope of the test section was adjusted to obtain uniform flow under initial steady conditions. An initial depth of flow of 0.25 in. was used. The water depth in the main reservoir was kept at 2.27 in. over the test section datum by means of a partial vacuum of 1.54 in. of water. The surface velocity of the initial flow was 21.07 in./sec and the velocity of the advancing jump 40.6 in./sec, with a final discharge over the test section of 0.242 ft³/sec. The steadiness of the depth behind the jump, from measurements at single points, was brought to within 0.005 in. The length of the steady region behind the jump reached approximately 12 in. The slope of the jump front was shown to occupy up to 2.5 in. in length. The grid scribed on the model in Fig. 11 represents inches longitudinally and tenths of inches vertically.

The upper photograph in Fig. 11 shows a constant depth along the wedge wall produced by the initial steady flow which moves to the right. The lower photograph shows the incident jump, with its front between stages 7 and 8, advancing to the right into the initial steady flow. The water line is clearly delineated except on the trough, where the falling water level makes the definition less certain. The position of the front is not clearly defined since the perspective view of the front itself covers the profile at the model wall. The front was taken at the intersection of the incident jump crest with the end of the profile at the wall. The turbulence of the water had only a small effect on the regularity of the depth distribution along the model wall.

The experimental results from a typical run and the theoretical aerodynamic results for the corresponding cases are shown in the graph of Fig. 12. Experimental depth distributions are measured directly from photographs such as the lower section in Fig. 11. The nondimensional ratio h/h_4 is then computed making the constant depth region nearest the leading edge coincide with the theoretical value. This permits a better evaluation of the deviations which occur in the variable region which follows. In the graph of Fig. 12, the abscissa for the experimental curve l/L represents the variable distance from the leading edge over the distance from the leading edge to the jump front. For the theoretical curve, x_{II} corresponds to the conical coordinate plane abscissa with the origin in the center of the variable region that limits at the sonic circle. The scales were adjusted to make the initial points of the variable regions and the positions of the incident shock and jump coincide for the two cases. Since,

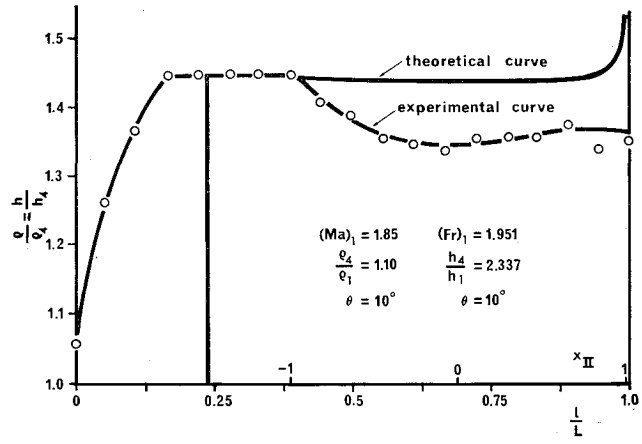

Fig. 12 Aerodynamic density and hydrodynamic depth ratio distributions along the walls of a wedge in supersonic motion, being struck by an incident shock wave and hydraulic jump, respectively.

through the application of the correlation, Mach and Froude numbers differ from each other, the linear proportions of the various regions in the interaction pattern result in differences in air and water.

The theoretical curve and the experimental curve of Fig. 12 lie within a deviation of 7%, except at the region of the front itself, where the deviation is larger. The experimental scatter reaches a maximum of approximately 8%.

A comparison between the theoretical and experimental curves in Fig. 12 shows that the trends that agree are the initial section of constant value, the decrease following it, and the increase up to the front.

The discrepancies are that no sharp discontinuity exists at the leading edge for the experimental case. Also, the decrease following the section of constant value is consistently larger, and the rise at the front is smaller.

These discrepancies can be partly explained by experimental deviations. The gradual rise of the water level at the leading edge of the model is caused by inertial, viscous, and surface tension effects. The smaller rise at the front in the experimental case is partly a consequence of the front of the incident hydraulic jump not being square but having an extended slope. Further sources of disagreement are that the theory was developed on a linearized basis considering a very weak incident shock with the properties of a sound pulse. This results in a flow pattern in which the incident shock always has a regular reflection at the deflecting wall, whereas experimental hydraulic analogy results show that a Mach reflection occurs for the corresponding flow conditions (see Figs. 6 and 7).

Conclusions

A general comparison of theoretical gasdynamic features with experimental interaction and diffraction patterns obtained by the hydraulic analogy shows that the principal theoretical assumptions are substantiated. The experimental pattern configurations also provide additional information on features that have not been predicted theoretically.

In case 1, a strong shock striking a supersonically traveling wedge with weak attached shocks, observed features include a strengthening at the kink in the attached hydraulic jump, the displacement of the centers of the circular disturbances inside the attached jump, and the weakening and breaking up of the incident jump at the model wall. The theoretical characteristic that was not apparent was a slight bend in the incident shock.

In case 2, a weak shock striking a supersonically traveling wedge with strong attached shocks, newly observed features

are the two straight segments intersecting at an angle on the attached hydraulic jump, a slight weakening at this intersection, and a straight disturbance line starting from the first break in the attached jump, followed by a patch disturbance. A Mach type reflection of the incident shock occurred instead of a regular reflection.

In case 3, a strong shock striking a stationary wedge at varying angles of incidence, practically all theoretical predictions were apparent. It was observed that the incident jump has an inflection point in its approach toward the expansion side of the wedge. In all three cases the contact discontinuity was not reproduced in visible form.

The experimental transient flow field distribution along the model wall, obtained for case 2, shows good correspondence in trend with the results from a linearized aerodynamic theory. The accuracy of the agreement is strongly affected by the limitations of the theory and by the characteristics of the experimental hydraulic flow. The comparison of experimental results with theoretical results through the correlation developed for this problem implies a linear distortion of the flow regions so that only corresponding regions must be analyzed simultaneously at any time. A discrepancy also affecting the distribution, and already mentioned in connection with the corresponding flow pattern configuration, is the occurrence of a Mach type reflection instead of a regular reflection of the incident shock at the deflecting wall, as predicted theoretically.

The hydraulic analogy to compressible gas flow has again proved its value as a means for the investigation of high-speed gasdynamics problems. It should be noted, nevertheless, that the theoretical conditions for the establishment of the analogy and the real experimental conditions impose serious restrictions on the analogy. Therefore, a successful application of the hydraulic analogy requires a sound knowledge of the many intervening factors and a careful interpretation of the results.

References

[1] Ippen, A. T., Harleman, D. R. F., and Crossley, H. E., Jr., "Studies on the validity of the hydraulic analogy to supersonic flow," Massachussetts Institute of Technology Hydrodynamics Lab., U. S. Air Force TR 5985, Parts I and II (May 1950), Part III (October 1950), Part IV (February 1952), and Part V (December 1952).

[2] Smyrl, J. L., "The impact of a shock wave on a thin two-dimensional aerofoil moving at supersonic speed," J. Fluid Mech. **15**, 223–240 (1963).

[3] Anderson, W., "Two problems of diffraction in gases," Ph.D. Thesis, Univ. of Bristol, England (1964).

[4] Fletcher, C. H., Taub, A. H., and Bleakney, W., "The Mach reflections of shock waves at nearly glancing incidence," Rev. Mod. Phys. **23**, 271–286 (July 1951).

[5] Guderley, K. G., *The Theory of Transonic Flow* (Pergamon Press, New York, 1962), Chap. VIII. 9, p. 241.